https://doi.org/10.5194/egusphere-2026-4213
Preprint. Discussion started: 27 July 2026

Towards more realistic calving simulations: the effects of subglacial hydrology on stochastic calving at Sermeq Kujalleq (Store Glacier), west Greenland.

Samuel J. Cook[1*], Iain Wheel[2], Nick Hulton[3], Poul Christoffersen[4], and Doug I. Benn[5]
[*]Corresponding author: Samuel Cook, samuel.cook@fau.de
[1]Institute of Geography, Friedrich-Alexander Universität Erlangen-Nürnberg, Erlangen, Germany
[2]Division of Biological and Environmental Sciences, University of Stirling, Stirling, UK
[3]Independent researcher, UK
[4]Institute for Marine and Antarctic Studies, University of Tasmania, Hobart, Australia
[5]School of Geography and Sustainable Development, University of St Andrews, St Andrews, UK

Abstract

Accurate modelling of long-term calving behaviour at tidewater glaciers remains a major challenge in glaciology, with existing methods being either overly computationally intensive, or too simplistic to capture observed calving behaviour. Building on previous work that showed the potential of a stochastic positional approach to modelling calving, we investigate how far a stochastic calving model can reproduce observed terminus dynamics and calving behaviour at Store Glacier (Sermeq Kujalleq), West Greenland, with and without coupling to a subglacial hydrology model. We show that the stochastic model is capable of accurately reproducing both qualitative and quantitative dimensions of calving at Store Glacier, while the inclusion of the subglacial hydrology increases calving volumes and produces the observed seasonal calving cycle. We conclude that simple hydrological parameterisations that leave the basal water pressure fixed in time cannot produce the full spectrum of observed calving behaviours of tidewater outlet glaciers.

1 Introduction

Mass loss from calving represents a major contributor to ice-volume loss globally, particularly from the two polar ice sheets, where calving and subaqueous melt represent nearly all mass loss in Antarctica and about 40% of mass loss in Greenland (Greene et al., 2022, 2024). As such, realistic representations of calving in glacier and ice-sheet models are a *sine qua non* for improving the accuracy of long-term simulations of these ice bodies and thereby providing better constraints on the timing and magnitude of sea-level rise globally (Li et al., 2023). However, existing methods for modelling calving are unsatisfactory: at one end, full-physics, explicit-fracture models such as the Helsinki Discrete Element Model (HiDEM) are far too computationally expensive to use at scale (Åström et al., 2013), whilst, at the other end, the simple rate-based functions usually employed in ice-sheet models (e.g. Choi et al., 2018; Edwards et al., 2021; Seroussi et al., 2024) rely on the case-by-case manual adjustment of a calving parameter ("tuning") and are unable to accurately reproduce the observed range of calving behaviour, especially once the model state diverges from the initial state for which the tuning was undertaken (Benn et al., 2026; Wheel et al., 2026). Other approaches have also been tried, e.g. the material-point method (e.g. Huth et al., 2021a, b) or linear elastic fracture mechanics (e.g. Jiménez and Duddu, 2018; Yu et al., 2017), but these either cannot be implemented in continuum models or run at the scale required to predict ice-sheet evolution. Fundamentally, the fracture mechanics that control calving are too computationally expensive to model explicitly at an ice-sheet scale, and too complex to reduce to simple deterministic rate functions. This longstanding problem has motivated attempts to reconceptualise calving and develop a computationally practical, reliable means of representing calving in continuum models. Benn et al. (2026) argued that the problem can be approached by leveraging observed self-organising behaviour of tidewater glaciers and ice shelves. These behaviours include the universal tendency of calving glaciers to form vertical terminal cliffs, stabilisation of calving fronts at pinning points and periods of rapid transition between stable positions, and calving event size distributions with consistent statistical properties (Åström et al., 2021, 2014; Benn et al., 2023, 2026). Importantly, all calving events fall into one of three statistical populations when size is plotted against frequency: power-law distributions for small, ice-cliff-scale events, and exponential or log-normal distributions for full-depth, ice-tongue-scale events. The power-law distributions reflect correlated calving events and self-organising criticality, whereas the exponential and log-normal distributions reflect uncorrelated events with underlying probabilities of occurrence (Benn et al., 2026). By combining the crevasse-depth-based calving algorithm (CD) of Todd et al. (2018) and Wheel et al., (2024a) with functions scaling the probability of calving to the state of stress in the ice, Benn et al. (2026) found that self-organising behaviours emerged spontaneously from the model, including calving-size distributions and different lengths of calving cycles for synthetic geometries representative of a Greenland tidewater glacier and an Antarctic ice shelf.

The model presented by Benn et al. (2026) adopted a provisional probability function based on theoretical considerations, and was not tested against real-world conditions. Important questions remain unanswered, including the degree to which the stochastic positional calving model works for real glacier geometries, and how the model parameters might vary depending on model formulation. Here, we address these questions by modelling the calving behaviour of Sermeq Kujalleq (Store Glacier), west Greenland, using the stochastic positional calving model implemented in Elmer/Ice with and without coupling to the subglacial hydrology model, GlaDS (Cook et al., 2021a; Benn et al., 2026). The uncoupled model exhibits self-organising behaviour, including the seasonal range of ice-front positions, spatio-temporal patterns of calving events, and statistical calving-size distributions, while the coupled model allows additional behaviours to emerge. Importantly, including coupling with subglacial hydrology affects calving frequency, both with regards to the effect on calving mechanics and as a driver for meltwater-plume melt rates at the calving front, and produces a seasonal calving cycle of calving without the need for mélange-induced backstress. The model is further tested in a comparative study of Sermeq Kujalleq (Store Glacier) and Sermeq Kujalleq (Jakobshavn Isbrae) in a companion paper (Wheel et al., in prep).

2 Study site

Sermeq Kujalleq (Store Glacier) is a large tidewater outlet glacier of the Greenland Ice Sheet in the central-west portion (70.4°N, 50.55°W) of the island (Fig. 1). The calving front is approximately 5 km wide with maximum ice thickness of ~600 m, and exhibits annual cycles of a few hundred metres of advance and retreat about a stable position that the glacier has occupied since at least 1948 (Catania et al., 2018; Weidick, 1995), due to pinning on a basal still and by constriction of the fjord walls. Annual velocities at the calving front reach up to 6 km a^{-1} (Joughin et al., 2018).

https://doi.org/10.5194/egusphere-2026-4213
Preprint. Discussion started: 27 July 2026

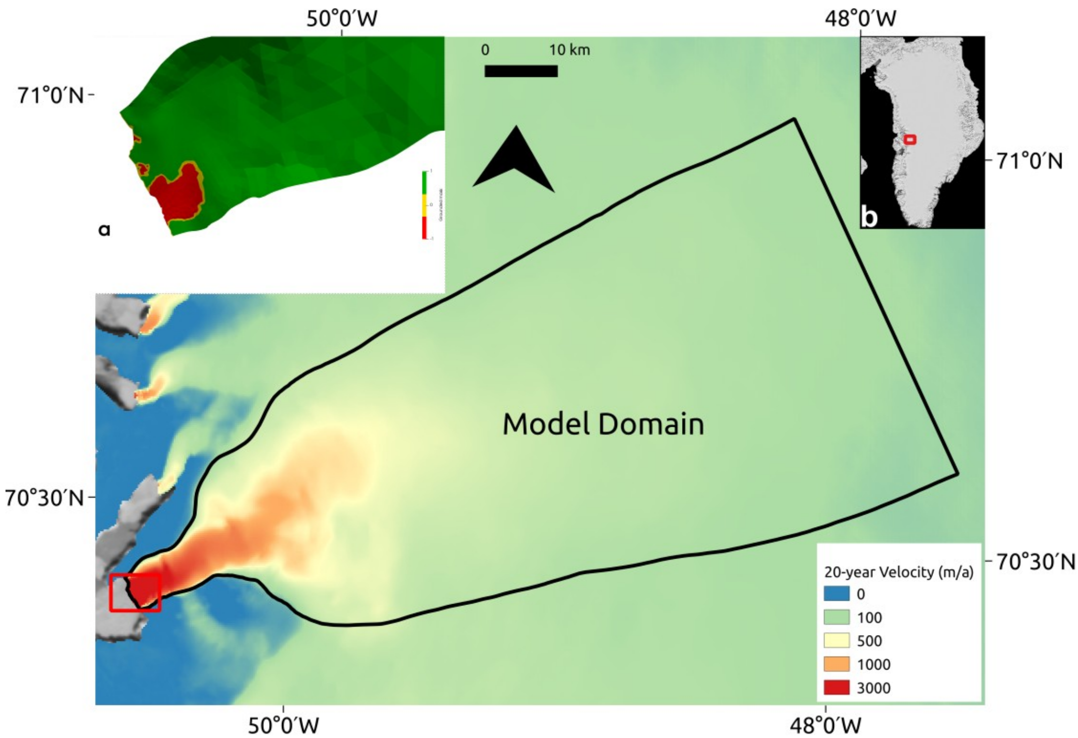

Figure 1: Model domain of Sermeq Kujalleq (Store Glacier). Background shows the 20-year velocity average (1995–2015) from the MEaSUREs dataset. Inset a shows an example of the grounded mask at the front (area shown by red box in the main figure), where red is ungrounded ice, yellow is the grounding line, and green is grounded ice. Inset b shows the location of the glacier within Greenland (red box).

3 Data and methods

The model domain, boundary conditions, and underlying data are identical to those in Cook et al. (2021a), specifically for the 2012 experiment. A summary is provided here, but the reader is directed to this publication and the references therein for full details.

3.1 Model setup

The model domain is defined by the 100 m a^{-1} velocity contour within the drainage basin of Store. This is meshed at 100 m near the calving front, coarsening to 2 km beyond 20 km inland from the initial calving front. A separate mesh is used for the subglacial hydrological modelling, extending inland from a short way beyond the initial calving front, meshed at 100 m resolution up to 20 km inland and then coarsening linearly to 2 km by the 100 km mark. All modelling is undertaken using the 3D, full-Stokes, open-source ice-flow model, Elmer/Ice (Gagliardini et al., 2013) and the implementation of the Glacier Drainage System (GlaDS) subglacial-hydrology model therein (Gagliardini and Werder, 2018; Werder et al., 2013). The model also implements meltwater plumes at the calving front driven by the discharge from the hydrological system, as well as using the 3D CD calving implementation from Todd et al. (2018) modified as described

https://doi.org/10.5194/egusphere-2026-4213
Preprint. Discussion started: 27 July 2026

below to represent stochastic calving. The system is fully coupled, with ice velocity used as an input for the hydrology, water pressure calculated by GlaDS feeding back to the ice velocity via a Coulomb sliding law (Gagliardini et al., 2007) and used as an input for the calving algorithm, and melt rates from the plumes being applied directly to the glacier terminus. No-slip conditions are specified at the lateral boundaries, whilst a constant velocity is specified at the inflow boundary. At the terminus, hydraulic potential is set to 0, following the argument laid out in Cook et al. (2020, 2021a). The model is forced using 2012 surface mass-balance (for the ice) and runoff (for the hydrology) data at 1 km resolution from RACMO 2.3p2 (van Wessem et al., 2018).

3.2 Model procedure

We follow a similar model relaxation procedure to that our previous work (Cook et al., 2021a), with some modification, as follows:

- Step 1: Steady-state simulation to obtain a converged temperature-velocity field.
- Step 2: Steady-state inversion from the results of Step 1 to obtain values for the friction coefficient at the base of the glacier using the 20-year velocity mosaic from MEaSUREs (Joughin et al., 2018).
- Step 3: Transient simulation lasting 1 year to initialise the subglacial hydrology, using the friction field obtained from Step 2 to provide a constant ice velocity. GlaDS is turned on, but not coupled to the overlying ice. Basal water system contains basally produced meltwater only. Glacier surfaces fixed and no calving.
- Step 4: Transient simulation lasting 4 years, using the hydrological system obtained from Step 3 to relax the coupled hydrology-plumes-ice system. Glacier surfaces allowed to relax. No calving.
- Step 5: Transient simulation lasting 1 day with all model components present and coupled to allow relaxation of the entire system. Calving is turned on.

This procedure adopts shorter relaxation periods than in Cook et al. (2021a) because our more recent work on tidewater glaciers has shown that such extensive relaxation times are unnecessary (Benn et al., 2026; Wheel et al., 2024b).

3.3 Stochastic calving implementation

We use the stochastic positional calving model as set out in Benn et al. (2026). In the original crevasse depth (CD) calving model, calving is predicted based on the depths of surface and basal crevasses calculated using the Nye-Jezek zero-stress assumption (Nick et al., 2010; Todd et al., 2018; Wheel et al., 2024a). In the stochastic model, we retain these equations, but it is important to note that these are no longer intended to represent physical crevasses. Rather, the functions are simply used to calculate the fraction of the glacier thickness that is under tensile stress, and thus should be regarded as a metric of stress.

A surface layer of tensile stress (d_s) occurs where $\sigma_1 > 0$ (1a)

and a basal layer of potential tensile stress (d_b) occurs where $\sigma_1 + P_w > 0$ (1b)

in which σ_1 is the principal stress (positive = extensional) and P_w is the water pressure within any potential fractures (Todd et al., 2018). From (1), depths of the surface and basal tensile

https://doi.org/10.5194/egusphere-2026-4213
Preprint. Discussion started: 27 July 2026

layers, d_s and d_b respectively, are calculated and used to define a *tensile depth ratio* $\underline{d}$:

$$\bar{d} = max\left(\frac{ds}{h}, \frac{ds+db}{H}\right) \tag{2}$$

where *h* is the freeboard and *H* is the ice thickness. In the original model of Todd et al. (2018) and Wheel et al. (2024a), calving was predicted to occur above a fixed value of $\bar{d}$. Here, we follow Benn et al. (2026) and scale the probability of calving to $\bar{d}$. First, we define a waiting time τ between calving events:

$$\tau = \tau_0 \exp(k(1-\bar{d})) \tag{3}$$

where τ_0 is the model timestep (1 day), and *k* is a scaling parameter. This exponential function is motivated by the observation that waiting times between calving events vary over about 5 orders of magnitude, from hours in high-stress environments such as the termini of fast-flowing Greenland tidewater glaciers to decades in low-stress environments such as steady state Antarctic ice shelves.The probability of calving occurring in a model timestep for a given value of $\bar{d}$ is:

$$p = 1 - \exp(-\tau_0/\tau) \tag{4}$$

The calving prediction is implemented using a modified form of the calving algorithm described by Todd et al. (2018). For each model timestep, inverted forms of equations (3) and (4) are used to define a threshold value of $\underline{d}$ above which calving will occur for the value of *p* that has been stochastically generated that timestep. Having established the threshold value of $\underline{d}$, the algorithm seeks areas of the model domain that satisfy the calving criterion. If no such areas exist, no calving occurs; if such an area isolates a region with a boundary along the ice front, that region is calved. The form of the functions dictates that, in any given timestep, calving is very likely to occur where $\underline{d}$ is close to 1 (i.e. if a tensile stress regime exists for most of the ice column), whereas calving is unlikely for lower values of $\underline{d}$ (where a smaller proportion of the ice column is under tension). Both the deterministic and stochastic variants of the model produce calving magnitude-frequency distributions described by:

$$n(S) = c_1 S^{-\alpha} \exp(-S/S_{01}) + c_2 \exp(-S/S_{02}) \tag{5}$$

where α has a value defined by universal fragmentation processes in brittle-elastic materials, *n* is the number of calving events of size *S*, c_1 and c_2 are constants, and S_{01} and S_{02} are the characteristic size intervals of specific fragmentation processes (Åström et al., 2014; Benn et al., 2026). These distributions are not an artefact of the probability function, but reflect the stress-based positional approach and have been shown for deterministic simulations (e.g. Benn et al., 2026; Wheel et al., in prep).

3.4 Model experiments

5

https://doi.org/10.5194/egusphere-2026-4213
Preprint. Discussion started: 27 July 2026

We run five experiments for this study (Table 1), each lasting three months, consisting of coupled and uncoupled model setups, winter and summer conditions, and varying the free parameter *k* in the stochastic calving function. In all experiments, GlaDS was used to provide water-pressure inputs for the friction law and discharge at the ice front for a plume model used to calculate submarine melting rates (Cook et al., 2021a; Slater et al., 2016). Melting undercuts the ice front, increasing stress on the subaerial part and increasing the probability of calving. In addition, in the *coupled experiments*, output from the GlaDS hydrology model was used to define P_w in equation 1b, so that evolving basal hydrology affects the depth of penetration of basal crevasses and hence the calving prediction. In the *uncoupled model experiments*, P_w is defined by the depth of the ice base below sea level. Although simple in form, the calving model allows a range of realistic behaviours to emerge, including frequent calving in high-stress regions, ice-front stability in low-stress regions such as pinning points, and sensitivity to melt-undercutting. We also note that, while the stochasticity of the model would ideally require an ensemble of simulations to be run, we do not do so here, both because of the computational expense and also because our main concern in this paper is to demonstrate that the model is capable of accurately reproducing general calving behaviour at Store and how this is affected by hydrology and *k* values, rather than trying to accurately reproduce a specific period of observed behaviour or an accurate projection of future behaviour.

Winter and *summer runs* used GlaDS hydrology forced by surface runoff in JFM and JJA 2012, as described by Cook et al. (2021a). Finally, values of the parameter k were chosen for comparison with uncoupled model studies of Jakobshavn Isbrae (*k* = 24; Wheel et al., in prep.) and optimizing fit between coupled simulations and observations of calving at Store Glacier (*k* = 20).

Table 1 - Model experiments undertaken as part of this study

Name	Period	k	Calving Coupled
StoreSK20C	Summer	20	Yes
StoreSK20U	Summer	20	No
StoreSK24U	Summer	24	No
StoreWK20C	Winter	20	Yes
StoreWK24U	Winter	24	No

4 Results

4.1 Comparison to calving observations at Store

We compare our model results to a time series of observed calving events at Store gathered using a terrestrial radar interferometer (TRI) at the terminus in July 2017 and to observed terminus positions in the MEaSUREs dataset between 2015 and 2022 (Black and Joughin, 2023), showing the small seasonal advance-retreat cycle that the terminus of Store undergoes

https://doi.org/10.5194/egusphere-2026-4213
Preprint. Discussion started: 27 July 2026

each year (Fig. 2). Full details of the TRI setup and results can be found in Cook et al. (2021b); here we present the overall calving record in the same style as the model results to aid comparison. We show three weeks of calving observations for the northern half of the terminus (Fig. 3), as the TRI did not adequately image the southern half, due to the presence of a large ice promontory in the centre of the calving front that occluded the instrument's view of the southern terminus until near the end of the field campaign. It should be borne in mind that the TRI only records subaerial calving volumes - any submarine loss is invisible to it - so volumes will be an order of magnitude lower than in the model.

Comparing terminus observations to the modelled positions, we can see that all of the model runs have final terminus positions that fall within the multi-year observed range of terminus positions (Fig. 2a). SK20C presents a marked retreat on the grounded, northern side of the terminus, in some places to just behind the most-retreated observed position, whilst the southern, floating part of the front advances to a similar position as the two winter simulations. The mean terminus position therefore retreats initially to near the minimal observed limit, before re-advancing (as one would expect from the minimal observed position if the calving front is behaving realistically) and stabilising throughout the middle of the simulation, then advances a little at the end. This complex behaviour will be discussed further below. SK24U stays within the observed limits throughout, but does not qualitatively match observed summer behaviour (a small retreat), instead having an initial advance of its mean terminus position, followed by a retreat, re-advance and stabilisation, leaving it more-or-less back where it started, suggesting that the depth-parameterised water pressure is not capable of generating fully realistic calving. Tracking the mean terminus position through time also shows, for the two winter simulations, the importance of having a modelled rather than parameterised basal water pressure, as WK24U advances a little beyond the observed limits with several large ice promontories forming and moving the mean position forwards. WK20C, however, maintains its mean position within the observed limits throughout, whilst still showing the appropriate qualitative behaviour of an overall winter advance. The modelled terminus positions are discussed further in the next section.

Turning to the TRI observations (Fig. 3), a comparison with the modelled distributions for the summer runs (Fig. 5b,d,f) shows very similar qualitative behaviour. Near the northern margin (y = 0), we observe and model quasi-continuous, small calving events. Towards the centre (y > 1500), both model and observations agree on larger, more episodic events. We do not expect a quantitative match, both because the TRI only records subaerial calving volumes, not total volumes, and because the stochastic nature of the calving function means that the model will never exactly reproduce any particular observed set of calving events. However, the combination of a generally good quantitative match in total amount of calving as shown by the terminus positions, combined with a qualitative match in the styles of calving, gives us confidence that the model is accurately reproducing long-term calving behaviour at Store.

https://doi.org/10.5194/egusphere-2026-4213
Preprint. Discussion started: 27 July 2026

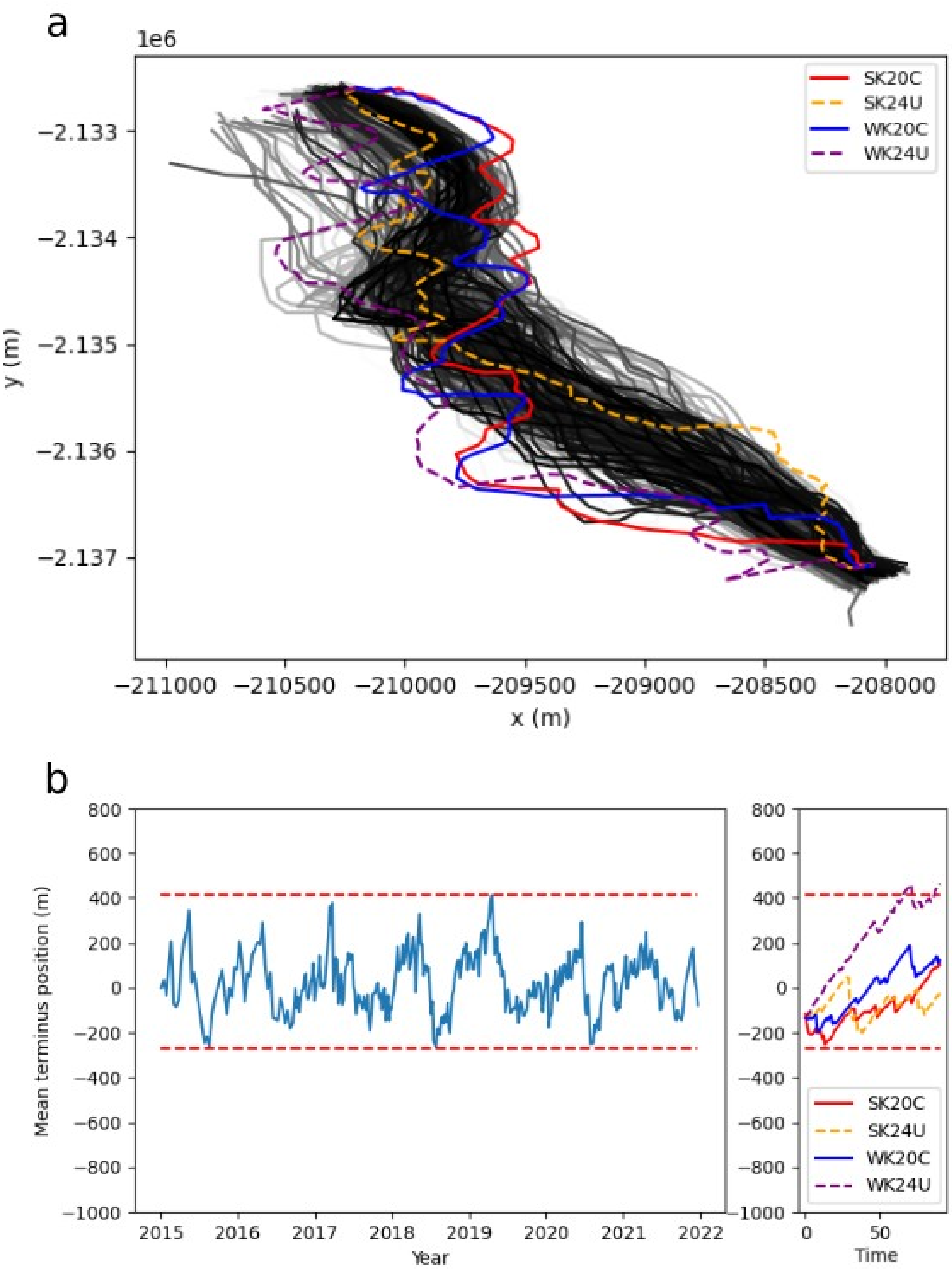

Figure 2: a. Observed Store terminus positions from Black and Joughin (2023) (grey-black lines) with final terminus positions from simulations (coloured lines). The axes scales are in EPSG: 3413 co-ordinates and note the y-scale is 1e6. b. Mean observed terminus position from observations (blue line, left) with maximum and minimum positions (dotted red lines) compared to mean modelled terminus positions (coloured lines, right). Position is relative to the front at the start of

https://doi.org/10.5194/egusphere-2026-4213
Preprint. Discussion started: 27 July 2026

the observational period in January 2015. Note we do not show the SK20U experiment in this figure because it is deliberately 'wrong' - the *k* value and the basal water pressure do not match - and therefore comparing it to observations provides no useful information about model performance. The performance of the four other runs is summarised in the preceding text and
255 **discussed extensively in the discussion.**

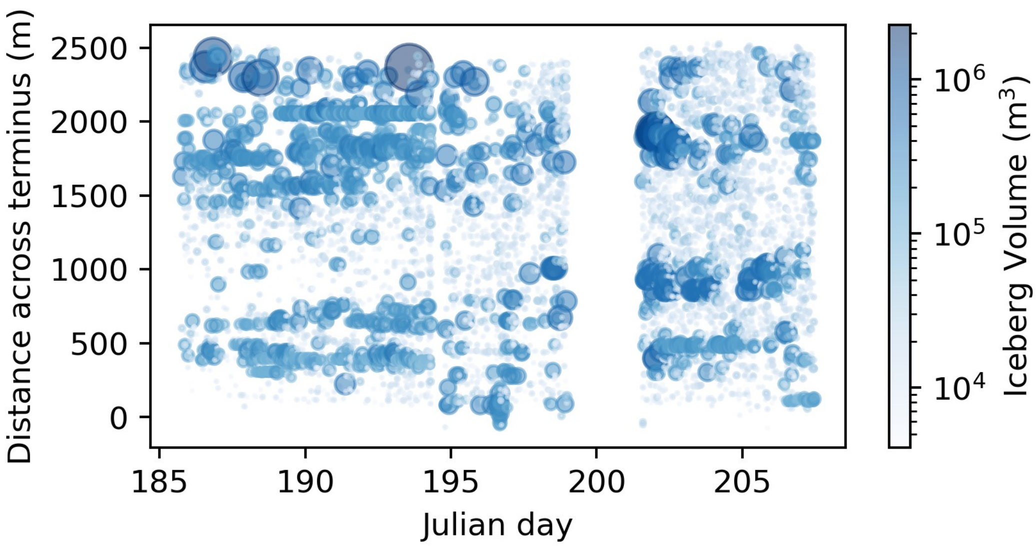

Figure 3: Observed calving volumes across the northern half of the terminus at Store during July 2017 from Cook et al. (2021b). 0 represents the northern margin, 2500 the centre of the calving front.

4.2 Terminus position

https://doi.org/10.5194/egusphere-2026-4213
Preprint. Discussion started: 27 July 2026

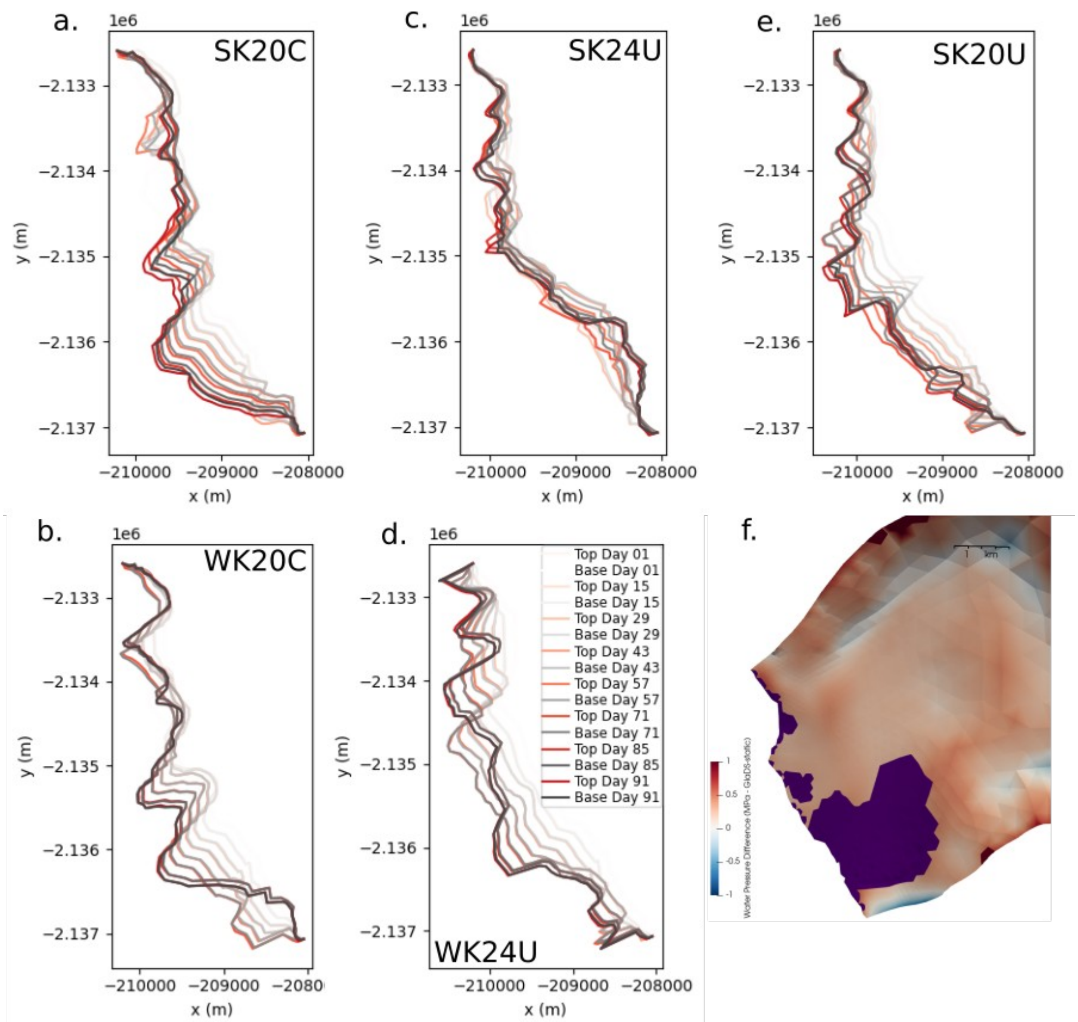

Figure 4: Terminus positions at the surface (reds) and base (blacks) over time for each simulation. a. SK20C, b. WK20C, c. SK24U, d. WK24U, e. SK20U. Axes co-ordinates for a-e are in EPSG: 3413, note y-scale is 1e6. Panel f. shows the difference in basal water pressure after one day of simulation between using GlaDS (SK20C) and the simple parameterisation from Todd et al. (2018) (SK20U).

We produce a range of behaviours in summer and winter at Store through the choice of different coupling and k values (Fig. 4). For coupled runs (using GlaDS to derive basal water pressure values), we model expected summer (small retreat) and winter (small advance) behaviour at Store with a k value of 20. The SK20C simulation (Fig. 4a) retreats by a few tens to hundreds of metres across the northern, grounded portion of the front, whilst advancing a few hundred metres in the floating, southern portion. WK20C (Fig. 4b), with a general advance of ~500 m along the terminus except in the far south and north, fits perfectly with the expected behaviour. For uncoupled (depth-parameterised basal water pressure) runs, a k value of 24 produces

https://doi.org/10.5194/egusphere-2026-4213
Preprint. Discussion started: 27 July 2026

similar behaviour. SK24U (Fig. 4c) is a little too stable, with some localised advance and retreat, but broadly within the stochastic range of summer behaviour, whilst WK24U (Fig. 4d) shows very similar outcomes to WK20C, though with more advance at the margins. SK20U (Fig. 4e) then shows the impact using the wrong k value for the model setup can have, as the lower k values makes the calving function too insensitive, leading to an overall advance of ~500 m across the entire front. This necessary difference in k value is the result of the higher water pressures in the lower few kilometres of the glacier produced by GlaDS compared to the simple depth parameterisation (Fig. 4f), regardless of season. Consequently, basal crevasses can penetrate farther into the ice and the k value needs to be reduced to modulate the sensitivity of the function appropriately.

4.3 Calving behaviour

We see consistent patterns of calving in all our simulations (Fig. 5), with the overall distribution obeying the universal power-law-exponential distribution theorised by Åström et al. (2021). We find best-fit parameters (black line in Fig. 7a) for this calving model to be α=1.0, c_1=50, c_2=6e^{-8}, s_{01}=1e^7, and s_{02}= 1e^8; the mismatch at the lower end of the distribution is due to the limits imposed by the mesh resolution perturbing the expected relationship. Calving events are most frequent in the northern half of the terminus and towards the southern edge. The south-central area, by contrast, calves much more episodically, but usually on a much larger scale. Interestingly, we do not see a clear summer/winter contrast in number of events, with 709 events on average in the two winter simulations, and 664 in the three summer simulations. However, we see a clear volumetric calving increase in summer (Fig. 7h): summer calving events are on average larger, with a mean volume of 2,356,222 m^3, compared to 1,952,125 m^3 for winter. This increase is also reflected and is indeed more pronounced at the median level (337,471 m^3 versus 233,604m^3, respectively), so is not simply the product of a few, very large events distorting the mean. This larger summer calving is though only barely visible when plotting the seasonal relative abundance (Fig. 7b), with winter and summer simulations showing very similar abundances across the curve, though summer, crucially, plots slightly above winter for volumes >10^5 m^3. That a seasonal signal is reflected in the model's calving behaviour is unsurprising, given the degree of difference between the summer and winter subglacial hydrological systems that determine the basal water pressures in the coupled simulations and the plume melt in all simulations (Fig. 6). The winter channelised system (Fig. 6b) is confined to the lower 5 km of the glacier, with a small amount of sheet discharge upstream, whilst the summer channel network (Fig. 6a) reaches ~40 km upstream, draining much higher sheet discharges. Basal water pressures are also much higher in summer than in winter for ~67% of the simulation, even in the most channelised part of the terminus, the northern margin (Fig. 6c). Readers interested in an exhaustive comparison of the subglacial hydrology of Store are directed to Cook et al. (2021a); we include this figure and note here purely to help explain the seasonality of calving in the model.

Furthermore, we also see major differences between the coupled and uncoupled simulations (Fig. 7, right column). Coupled simulations show considerably higher total abundances and calving volumes over time, despite the three uncoupled simulations including two summer runs that should bias the uncoupled results towards larger calving events. However, what is very clear from the relative abundances (Fig. 7c) is that uncoupled simulations have relatively fewer

https://doi.org/10.5194/egusphere-2026-4213
Preprint. Discussion started: 27 July 2026

larger events - the mean calving event in a coupled simulation is nearly 2 times bigger than in an uncoupled simulation (2,941,657 m^3 compared to 1,696,534 m^3) - which links to the more static terminus positions described for the summer uncoupled simulations above. Fully coupling GlaDS to the calving function via the basal water pressure therefore seems to be a key ingredient in reproducing observed calving behaviours and thus terminus positions.

We also see evidence in the model results for calving induced by plume melt and calving cascades (Fig. 8). In both SK20C and SK20U we see consistent plume melt at a location across tens of timesteps, which strengthens and then stops suddenly as the result of a large calving event happening in that sector. Given the complexity of the model, we cannot definitively state that this is a causal relation, but we contest that the repeated coincidence seems otherwise overwhelming. Similarly, the fact that a single smaller calving event on the southern half of the terminus in SK20C (Fig. 7b) leads to a sequence of other mid-size and small calving events in the same region in its immediate aftermath seems to us a pattern that clearly fits the definition of a calving cascade. Both of these emergent behaviours strongly indicate the coupled model is exhibiting a full range of calving behaviours.

https://doi.org/10.5194/egusphere-2026-4213
Preprint. Discussion started: 27 July 2026

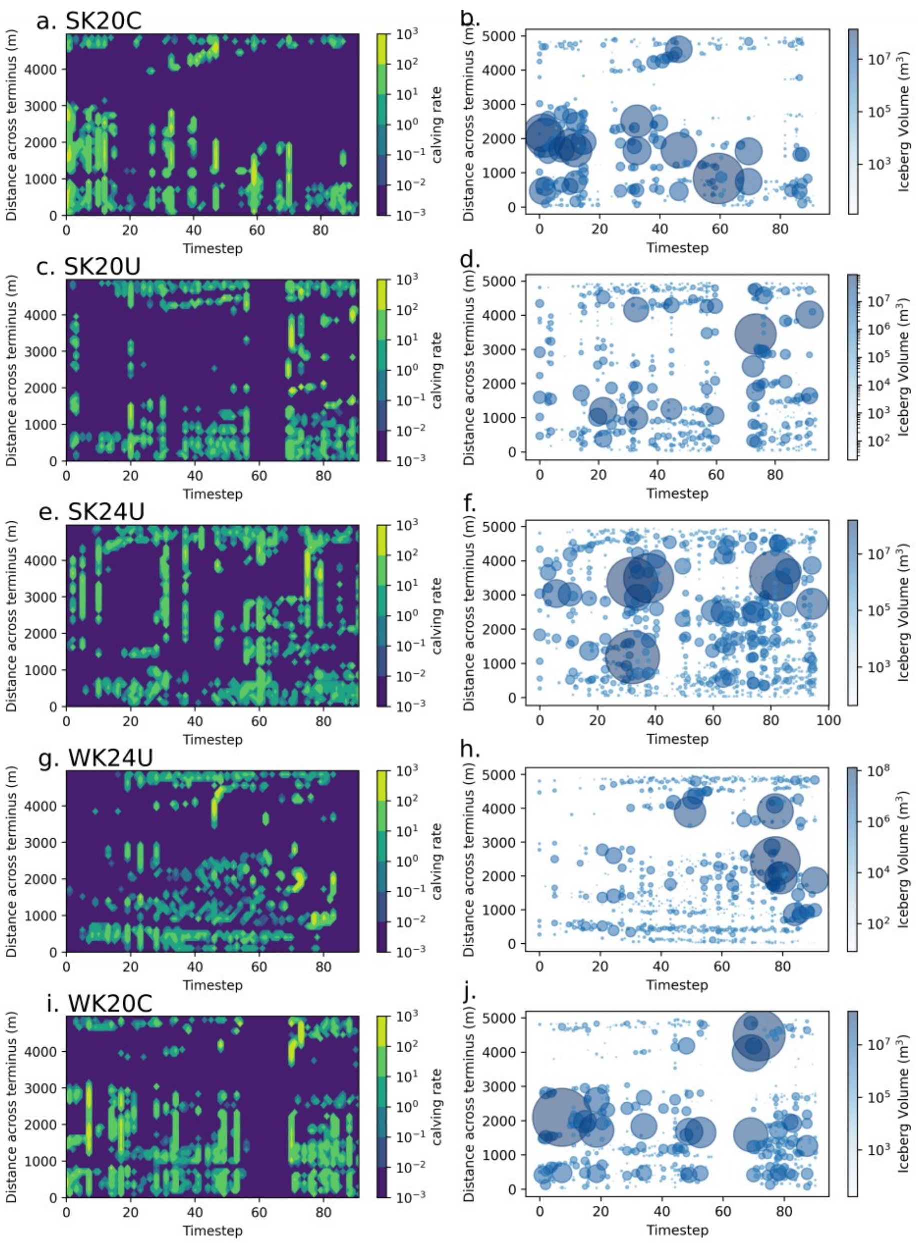

Figure 5: Calving rate (left) and iceberg volumes (right) by time and position (the northern margin is 0) across the terminus for each simulation. a. and b. SK20C, c. and d. SK20U, e. and f. SK24U, g. and h. WK24U, i. and j. WK20C. The calving rate is the length of ice removed at that point at that timestep.

https://doi.org/10.5194/egusphere-2026-4213
Preprint. Discussion started: 27 July 2026

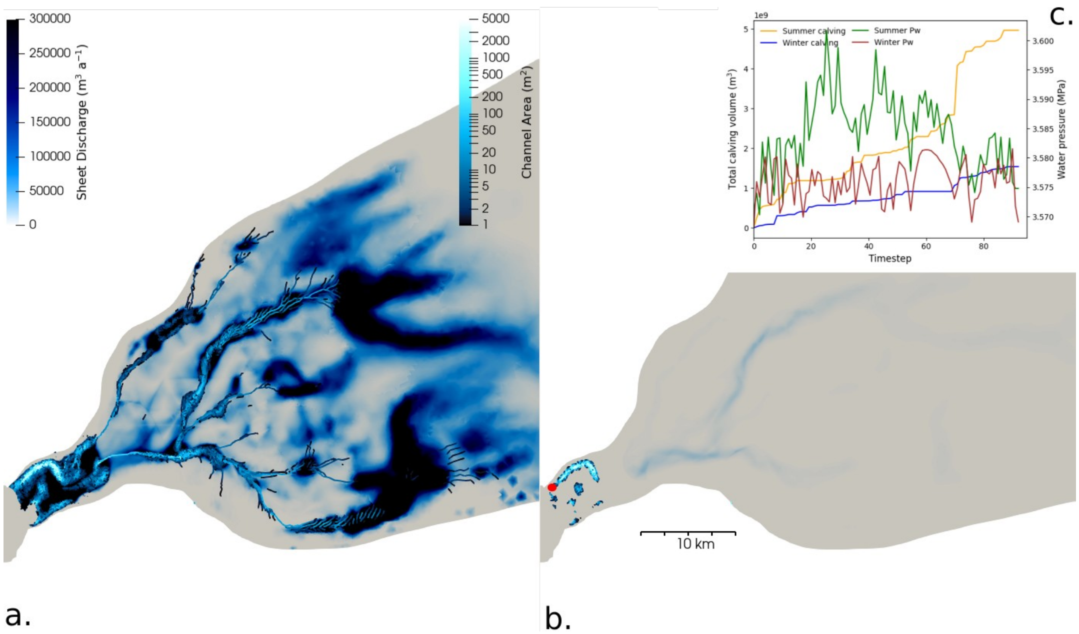

335 **Figure 6: a. Maximum extent of Store summer hydrological network from SK20C (day 66), b. Winter extent of hydrological network from WK20C. Both panels show channel cross-sectional area, plotted as a scalar for each channel segment (an edge in the mesh), overlaid on sheet discharge. Inset c. shows water pressure at base at location of red dot in panel b. for both winter (WK20C) and summer (SK20C) plotted against the respective cumulative calving volumes.**

https://doi.org/10.5194/egusphere-2026-4213
Preprint. Discussion started: 27 July 2026

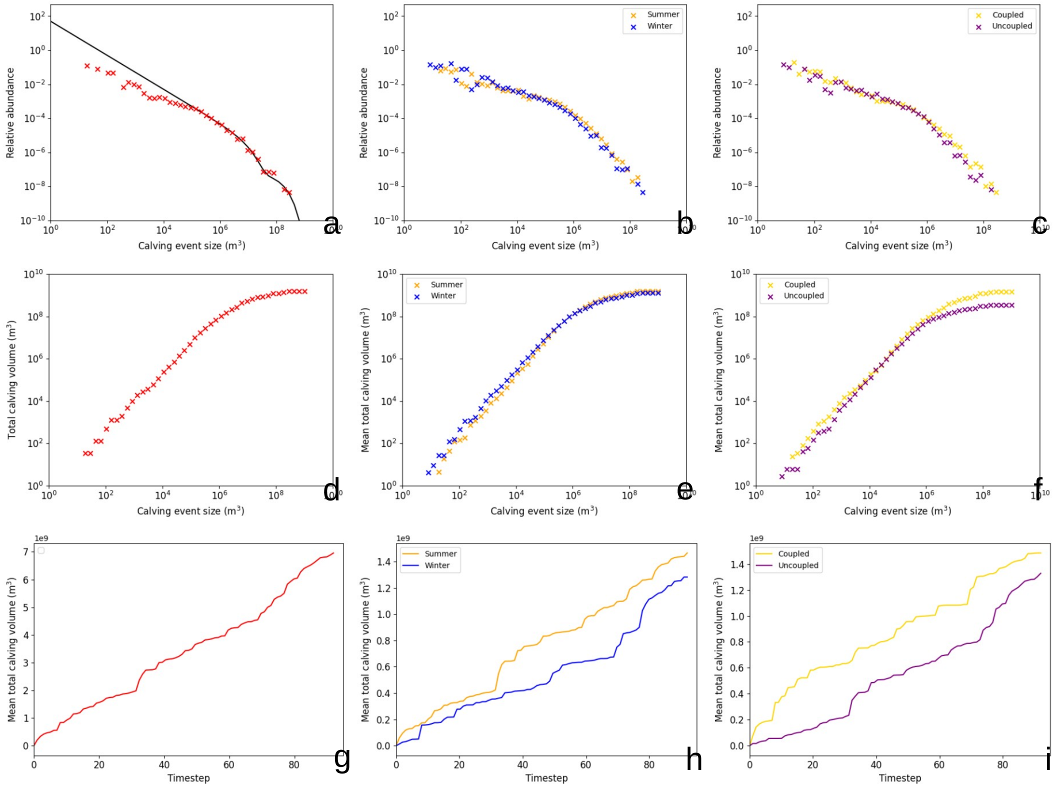

340 **Figure 7: Top row: relative abundance, middle row: total abundance, bottom row: mean cumulative calving volume. Left column: for all simulations, middle column: summer-winter comparison, right column: coupled-uncoupled comparison**

https://doi.org/10.5194/egusphere-2026-4213
Preprint. Discussion started: 27 July 2026

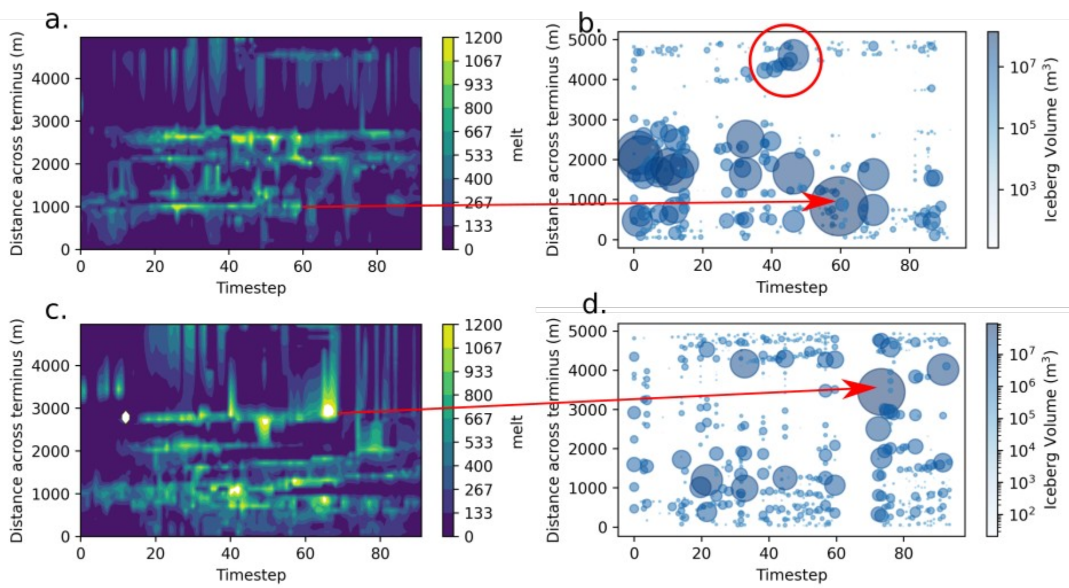

Figure 8: Plume melt across the terminus (left) and iceberg volumes (right) for SK20C (a., b.) and SK20U (c., d.). Red arrows show clear examples of sustained melting in one location leading to a calving event. Red circle shows a substantial calving cascade, as one event leads to a number of related events in the same location.

5 Discussion

5.1 Model richness

The main outcome of this paper is that including an explicit representation of subglacial hydrology in our model is crucial in improving the realism of our simulations of Store. We show the fully coupled stochastic-calving-GlaDS-plumes model is able to reproduce calving behaviour at Store that is consistent with observations: quasi-continuous small events on the grounded northern side of the terminus and at the southern margin, larger, more episodic events in the floating centre and south (Fig. 5). This shows the model is able to reproduce both main observed calving styles at Store and other tidewater termini: small-scale serac failure and large-scale, buoyancy-driven full-thickness calving (Cook et al., 2021b; Fried et al., 2018; Goliber and Catania, 2024), with the former dominating in the grounded northern sector and the latter in the ungrounded southern sector (Cook et al., 2021b). With k = 20, we are able to produce small summer retreats and winter advances, with both more and larger calving events in summer and fewer and smaller calving events in winter (Fig. 4). The magnitude-frequency distribution of the resulting icebergs (Fig. 7) follows the expected power-law-exponential model, with a more pronounced exponential bump when GlaDS is used as the source for basal water pressure values in basal crevasses. We also see what is almost certainly plume-caused calving, as well as calving cascades in the model output (Fig. 8). This is a level of richness in reproducing the behaviour of a tidewater glacier that, to our knowledge, is unparalleled.

5.2 Comparison to observations

The observational calving record for the northern half of the terminus at Store (Fig. 2) shows

https://doi.org/10.5194/egusphere-2026-4213
Preprint. Discussion started: 27 July 2026

remarkable similarities to modelled calving at Store using the stochastic calving function. We see the vast majority of larger events in both only occurring beyond ~1500 m from the northern margin, with quasi-continuous smaller events closer to the margin (Fig. 5, 9). Both observations and modelling also show strong clustering of calving events in both time and space - the former likely due to hydrologically mediated pressure pulses at the bed, the latter due to melt undercutting by plumes. This is strong evidence that the tensile-stress-based stochastic calving function is capable of accurately reproducing the qualitative aspects of real-world calving behaviour at Store. We also see a good quantitative match in the integrated impact of calving on terminus position (Fig. 1) for the four simulations with k values that match their basal-water-pressure fields. However, only WK20C produces both a strong quantitative and qualitative match, with mean terminus position remaining within the observed limits throughout the simulation. The uncoupled equivalent - WK24U - advances a little too far, showing that the explicit modelling of the basal water pressure with GlaDS is necessary to match observations at Store. SK24U, meanwhile, although the mean terminus position falls within the observational limits, does not show any retreat, meaning that it fails to qualitatively match expected summer behaviour, further underlining this point. SK20C presents the most complex picture: the northern half of the terminus retreats as expected within observational limits, while the south advances, which is contrary to expectations. This is due to the complex nature of the terminus at Store (part-grounded, part-floating) and how it interacts with the stochastic calving implementation. Only the grounded part of the terminus feels the basal water pressure produced by GlaDS, hence we see retreat here unlike in the uncoupled simulations (it is also notable that WK20C shows much less advance in the north than the uncoupled simulations for the same reason) due to the higher water pressures produced by summer melt runoff. On the southern side, the floating part of the tongue experiences a constant water pressure defined by the bathymetry and is therefore calving based solely on its position and the luck of the stochastic draw. With our simulation length being relatively short, it is therefore unsurprising that we see advance in the ungrounded south where larger infrequent calving is observed. We expect if the simulation SK20C were to continue a large calving event would occur in keeping with the observed terminus limits (Fig. 2). Some deviation from the observations is expected from the inherent unpredictability of a stochastic model on short timescales: if we had run the simulation for longer, the stochastic p-values would even out and the south side would have calved back and retreated. We are further confirmed in this interpretation by the abovementioned strong qualitative and quantitative match with observations provided by WK20C, strongly suggesting the model is capturing realistic calving behaviour at Store. Compared to this, we argue that exactly matching observed terminus positions, especially given the short runtimes of the simulations, is secondary, as this can be achieved by calibration of the calving function if desired, whilst the correct calving styles in the correct places cannot (Wheel et al., 2026). It is impossible for a simple calving function to capture exact calving events but we show the stochastic model produces both the observed calving styles and displays the observed limit cycle (Benn et al., 2026). As a final point, we also note that SK20C is the only summer simulation to show a retreat of the grounded northern terminus, thus it is the only simulation to display that fundamental aspect of summer terminus behaviour at Store.

5.3 Model coupling and seasonality

https://doi.org/10.5194/egusphere-2026-4213
Preprint. Discussion started: 27 July 2026

We particularly wish to highlight that the differences in calving caused by (not) using GlaDS are considerably larger than the seasonal summer-winter differences (Fig. 7) and produce a more realistic set of terminus positions (Fig. 4). The difference is due to the higher basal water pressures produced by inclusion of GlaDS (Fig. 4f), increasing $\underline{d}$ near the terminus where water pressure is high and therefore leading to more calving.This mechanism explains why k has to be reduced to dampen the sensitivity of the stochastic calving function. Preliminary tests showed that using higher k values with GlaDS led to uncontrolled retreat. The coupled-uncoupled differences are clearly visible in all three of relative abundance (Fig. 7c), total abundance (Fig. 7f), and cumulative calving volume over time (Fig. 7i). Coupled simulations have more calving at all points in the total abundance curve, with relatively more calving especially in the middle of the distribution (events of volumes 10^4-10^6 m^3). The most striking and intuitive difference can be seen in the cumulative calving curves, however, with coupled simulations having, on average, events nearly two times greater in volume, though the median is very similar, suggesting that it is the rare, large summer events that are driving this difference. Interestingly, though, coupled simulations have a smaller number of events on average - 510 versus 796 - which is a product of the functioning of the calving algorithm: as each location can only have one calving event per timestep, more large events inevitably leads to fewer smaller events, pushing down the overall count. This also explains the difference in the relative-abundance curves and in the pattern of terminus positions (Fig. 4), as discussed further below. That all of this comes from driving calving with modelled basal water pressures, rather than assuming that water pressure throughout the glacier is determined by water depth at the terminus, underlines the importance of this process at tidewater glaciers and the need to include it in models.

We do, though, still see some seasonal differences in calving. Most obviously, there is simply more calving in the summer simulations than in winter, with events that are, on average, 20% larger. In the coupled simulations, this is because GlaDS, responding to the high surface meltwater inputs, produces much higher basal water pressures than in winter (Fig. 6c). In the uncoupled simulations, though, there is no seasonal difference in basal water pressure, so we can also see the impact of the warmer prescribed background fjord field, more active meltwater plumes, and ice mélange presence/absence. While this affects the absolute amount of calving, the relative and total abundances (Fig. 6b and e) are much more similar between winter and summer. The relative lack of difference between summer and winter in terms of relative and total abundance can also be ascribed to the short lengths of the simulations in this paper; we would expect the differences to be clearer over 6-12 months. All these seasonal differences, though, are modest compared to those induced by coupling or uncoupling GlaDS with the calving function; indeed, Fig. 5 shows that SK20C and WK20C, the two coupled simulations, generate far more larger events on the northern side of the terminus than the uncoupled simulations, particularly in the 1000-3000 m range (i.e. 1-3 km in, starting from the northern edge). As this is the area most affected by switching between GlaDS and parameterised water pressures in the calving function, this is a key marker of the effect of changing the source of the basal water pressure field.

Further supporting our argument about the relative importance of coupling compared to seasonality, pronounced seasonal terminus patterns were only observed when using GlaDS coupling (Fig. 4). Both the coupled and uncoupled winter simulations show a slightly advancing

https://doi.org/10.5194/egusphere-2026-4213
Preprint. Discussion started: 27 July 2026

terminus (Fig. 4b,d) but only the coupled simulation showed a summer retreat pattern on the northern side where the ice feels the water pressure change (Fig. 4a). The uncoupled summer simulations remained stable (Fig. 4c) or even advanced (Fig. 4e). This is fundamentally driven by the larger number of larger calving events in the coupled simulations, showing that our model is able to reproduce observed terminus positions and behaviour at Store (Cook et al., 2021b) as a result of accurately capturing the underlying physical mechanisms, rather than due to the manual adjustment and overfitting of the calving function to observations.

We therefore further suggest that the seasonal effect on calving usually attributed to ice mélange (Crawford et al., 2024; Xie et al., 2019), and included in our winter simulations following Cook et al. (2021a), could be partially explained by the concomitant changes in the subglacial hydrology, basal water pressure, and plume activity. Whilst we cannot exclude that mélange has a stabilising effect on the terminus, we contend that it is likely overestimated when the influence of the wider hydrological changes are not currently included in most calving studies (e.g. Wheel et al., 2024b; Benn et al., 2026). However, more work is required to confirm this hypothesis. We argue, regardless of whether this should prove to be the case, that this underscores the importance of including more sophisticated representations of subglacial hydrology in models of calving glaciers and, ultimately, in ice-sheet models.

5.4 Plume-driven calving

Two examples from the model output of consistent plume melting in one location directly leading to calving events are shown in Fig. 8. This would be wholly in line with theoretical and observational considerations: as strong plumes melt backwards, parts of the front lose support both laterally and vertically, leading to them being more vulnerable to calving. Although the complexity of the model makes direct comparisons difficult, we are confident the model is capturing a real feedback. This is further strengthened by small-scale serac calving being clearly visible in the magnitude-frequency distributions (Fig. 7, top two rows), showing that the model is capable of modelling this style of event, as well as clear undercutting from plume melt in the affected areas being visible (Fig. 9). At the same time, we should not overstate the importance of this process: there are far more occasions where plume melting, even concentrated in one location over multiple timesteps, does not seem to bring about a major calving event. Though, of course, it is very likely that plume melting contributes, if not always obviously, to a great many of the calving events that take place in the model. Disentangling the exact extent of this would require additional simulations that are beyond the scope of this study, but the fact that the model is seemingly capable of including this process is, we argue, a hallmark of its success in reproducing real calving fronts (e.g. Bézu and Bartholomaus, 2024; Cook et al., 2021b; Fried et al., 2018; Goliber and Catania, 2024; Walter et al., 2020).

https://doi.org/10.5194/egusphere-2026-4213
Preprint. Discussion started: 27 July 2026

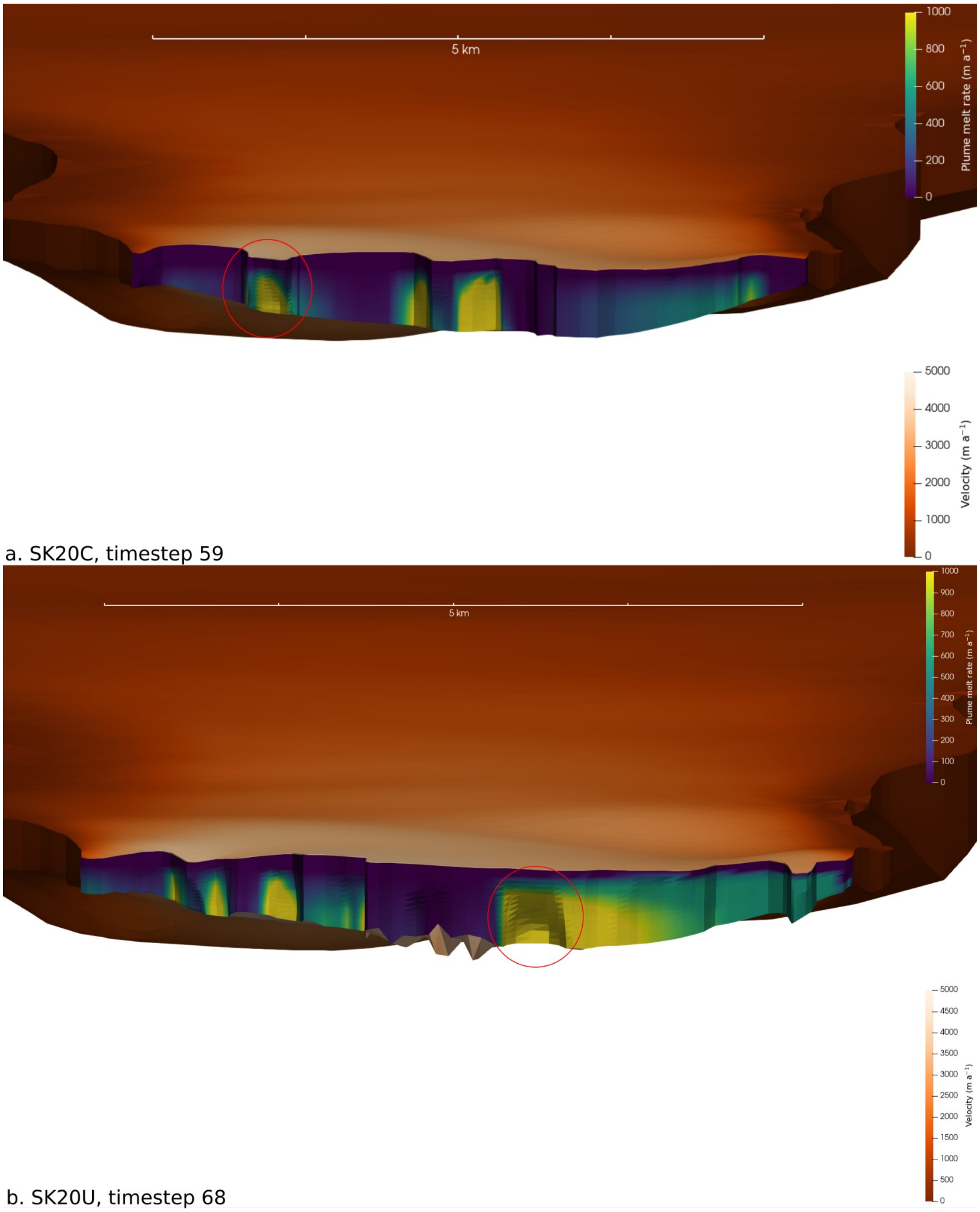

Figure 9: Plume undercutting (red circles) in both SK20C (a.) and SK20U (b.). These areas generate the calving events shown in Fig. 8 over the following timestep(s).

5.5 Calving styles

https://doi.org/10.5194/egusphere-2026-4213
Preprint. Discussion started: 27 July 2026

As a corollary of the main hydrological thrust of this paper, we also show the effectiveness of the stochastic calving function from Benn et al. (2026) in reproducing real-world tidewater-glacier behaviour. Of particular importance for the latter, we demonstrate that k=24, the preferred value of k in the setup without hydrology in Wheel et al. (in prep), works for our uncoupled setup here, and that k is therefore not dependent on model domain or small changes in model setup. Incorporating GlaDS necessitates reducing k to 20; this is a useful indication of the sensitivity of k and the range of values to explore for other model setups. In particular, this seems an indication that any finite-element model using a similar implementation of the stochastic calving function at a resolution of ~100 m at the terminus is very likely to have a k value in a similar range to that explored here (20-24). The different k values for the two model setups highlight the need to "calibrate" simple calving functions when separate processes are captured (the inclusion of subglacial water pressure). This is distinct from the manual adjustment ("tuning") often used to fit the output to observations (Wheel et al., 2026).

The simulations presented here also allow us to discuss some features inherent to the stochastic calving function that are worth noting. Firstly, our best-fit parameters for the combined relative-abundance curve (Fig. 7a) - α=1.0, c_1=50, c_2=6e^{-8}, s_1=1e^{7}, and c_2= 1e^{8} - do not align perfectly with those presented in Åström et al. (2021) or Benn et al. (2026), but, apart from α, the other parameters are expected to be site-dependent, reflecting particular waiting-time distributions. The important point is that our calving distributions fit the power-law and exponential curves produced by this statistical model, reinforcing previous observational work that calving can be considered a stochastic process and that these calving distributions are universal (Åström et al., 2021; Benn et al., 2026). Importantly, our α, which should be ~1.2 from theoretical and observational considerations (Benn et al., 2026), is within a reasonable margin of error. The fact that the other parameters vary is an illustration of both the natural variability of calving fronts - we, after all, only model a total of 15 months of calving activity in this paper - and also nicely illustrates the need for further work on this topic.

Finally there are periods of the simulations where calving does not occur, particularly around timestep 60 in SK20U (Fig. 3c) and WK20C (Fig. 5i). This is not a model or calving functionartefact but rather a representation of a real-world pattern where the terminus is stable, as seen in observations (Fig. 2a). During these periods, regardless of the p value generated in the stochastic calving function, the stress field of the glacier must be stable.

5.6 Future work

Along with Benn et al. (2026) and Wheel et al. (in prep), this paper should be considered a proof of concept showcasing the capability of the stochastic CD function to represent accurate calving styles across the terminus of Store. Across the three papers, we lay out the theoretical basis for a stochastic approach to modelling calving, show it reproduces observed styles and patterns of calving well in both synthetic and real settings, and explore some of the related issues, such as the sensitivity of k and the impact of including explicit modelling of subglacial hydrology. There is clearly, however, much work remaining to be undertaken in this direction. Future work will have four principal aims:

- Testing and validating the form of the stochastic calving function against observations of the fluctuations of calving fronts for a large sample of glaciers
- Testing the ability of the function to reproduce calving effectively at a wider range of real

https://doi.org/10.5194/egusphere-2026-4213
Preprint. Discussion started: 27 July 2026

glaciers, including Antarctic ice shelves and non-Greenland tidewater glaciers

- Devising a simpler version of the function that could be implemented in a vertically integrated, continuum-based ice-sheet model
- Developing the best way to include subglacial hydrology in calving calculations in ice-sheet models, either through coupling (as here) or by including an improved parameterisation directly in the calving function. This may not be a one-size-fits-all approach: simpler hydrology models may suffice for Antarctica, where surface melt is very limited, whilst Greenland may require a more complex solution, as surface melt is much higher and the subglacial hydrology evolves seasonally.

We should also note that the model presented in this paper does, of course, suffer from limitations. We do not model the fjord beyond providing a static seasonal (summer/winter) background temperature-salinity field for the plume model, which means we are missing a potentially important additional control on calving. Adding explicit fjord modelling may, however, be a complexity bridge too far if one wishes to retain a reasonable degree of computational efficiency and is not currently included in plans for future work. We are also fundamentally unable to resolve the smallest calving events, due to the limit imposed by the mesh resolution, again for computational reasons, perturbing the smaller end of our iceberg distributions (Fig. 7a). Due to the model complexity, we also cannot establish definite causal links between the different processes in all cases, though, as argued above, the alternatives require assuming an improbably high degree of coincidence in model behaviour. Finally, we would like to emphasise that the stochastic calving function remains a work in progress and refinements will be made in the coming years, but even in its current form the emerging calving dynamics from the model are strikingly similar to those observed.

6 Conclusion

By implementing a stochastic calving function in the previous coupled calving-subglacial-hydrology-meltwater-plumes model of Store, we are able to reproduce realistic terminus and calving behaviour at the glacier. Our iceberg distributions fit the expected statistical relationship and a seasonal advance-retreat pattern of the expected magnitude emerges naturally from the model. We show that taking basal water pressure values from GlaDS compared to a simple depth-dependent parameterisation increases overall calving, improves the modelled range of terminus positions, and produces a seasonal variation in calving. The inclusion of the subglacial hydrology required a change in k value in the stochastic calving function as different processes were being captured. We argue that calving functions should only be calibrated on a model-by-model basis in order to capture missing physics or processes, rather than the timeframe or site-specific “tuning” that has been commonplace that fits the calving function to a particular glacier state. Overall, this paper demonstrates the importance of including explicit representations of subglacial hydrology in models of tidewater glaciers.

Competing interests

One of the authors is a member of the editorial board of *The Cryosphere*.

Acknowledgements

This work is from the DOMINOS project (NE/006605/1), a component of the International

https://doi.org/10.5194/egusphere-2026-4213
Preprint. Discussion started: 27 July 2026

Thwaites Glacier Collaboration (ITGC). ITGC Contribution No. ITGC-177**.** SC would like to further acknowledge funding from the DeLIGHT project. This work is from the GIANT project, funded by the Advanced Research + Invention Agency (ARIA) Forecasting Tipping Points Programme (GIANT project; SCOP-PR01-P028). GIANT Contribution No. GIANT-002.

Data availability

All simulation results, code and data used in this paper are available on Zenodo at 10.5281/zenodo.21336520. The full dataset of results is, however, too bulky to upload but can be obtained by contacting the authors.

Author contributions

SC, DB, and IW designed the study and experimental setup. SC ran the simulations. SC analysed the data with help from IW. SC wrote the paper with input and comments from IW and DB. PC and NH assisted with the gathering and analysis of the TRI data.

References

Åström, J., Cook, S., Enderlin, E. M., Sutherland, D. A., Mazur, A., and Glasser, N.: Fragmentation theory reveals processes controlling iceberg size distributions, J. Glaciol., 67, 603–612, https://doi.org/10.1017/jog.2021.14, 2021.

Åström, J. A., Riikilä, T. I., Tallinen, T., Zwinger, T., Benn, D., Moore, J. C., and Timonen, J.: A particle based simulation model for glacier dynamics, The Cryosphere, 7, 1591–1602, https://doi.org/10.5194/tc-7-1591-2013, 2013.

Åström, J. A., Vallot, D., Schäfer, M., Welty, E. Z., O'Neel, S., Bartholomaus, T. C., Liu, Y., Riikilä, T. I., Zwinger, T., Timonen, J., and Moore, J. C.: Termini of calving glaciers as self-organized critical systems, Nat. Geosci., 7, ngeo2290, https://doi.org/10.1038/ngeo2290, 2014.

Benn, D. I., Todd, J., Luckman, A., Bevan, S., Chudley, T. R., Åström, J., Zwinger, T., Cook, S., and Christoffersen, P.: Controls on calving at a large Greenland tidewater glacier: stress regime, self-organised criticality and the crevasse-depth calving law, J. Glaciol., 1–16, https://doi.org/10.1017/jog.2023.81, 2023.

Benn, D. I., Wheel, I., Christoffersen, P., Åström, J., Cook, S. J., Luckman, A., Nick, F., Hulton, N., Hewitt, I., and Bassis, J.: Calving laws and where to find them, J. Glaciol., 72, e22, https://doi.org/10.1017/jog.2026.10128, 2026.

Bézu, C. and Bartholomaus, T. C.: Greenland Ice Sheet's Distinct Calving Styles Are Identified in Terminus Change Timeseries, Geophys. Res. Lett., 51, e2024GL110224, https://doi.org/10.1029/2024GL110224, 2024.

Black, T. E. and Joughin, I.: Weekly to monthly terminus variability of Greenland's marine-terminating outlet glaciers, The Cryosphere, 17, 1–13, https://doi.org/10.5194/tc-17-1-2023, 2023.

Cassotto, R. K., Burton, J. C., Amundson, J. M., Fahnestock, M. A., and Truffer, M.: Granular decoherence precedes ice mélange failure and glacier calving at Jakobshavn Isbræ, Nat. Geosci., 1–6, https://doi.org/10.1038/s41561-021-00754-9, 2021.

Catania, G. A., Stearns, L. A., Sutherland, D. A., Fried, M. J., Bartholomaus, T. C., Morlighem, M., Shroyer, E., and Nash, J.: Geometric Controls on Tidewater Glacier Retreat in Central Western Greenland, J. Geophys. Res. Earth Surf., 123, 2024–2038, https://doi.org/10.1029/2017JF004499, 2018.

Choi, Y., Morlighem, M., Wood, M., and Bondzio, J. H.: Comparison of four calving laws to model Greenland outlet glaciers, Cryosphere Discuss., 1–18, https://doi.org/10.5194/tc-2018-132, 2018.

Cook, S. J., Christoffersen, P., Todd, J., Slater, D., and Chauché, N.: Coupled modelling of subglacial hydrology and calving-front melting at Store Glacier, West Greenland, The Cryosphere, 14, 905–924, https://doi.org/10.5194/tc-14-905-2020, 2020.

Cook, S. J., Christoffersen, P., and Todd, J.: A fully-coupled 3D model of a large Greenlandic outlet glacier with evolving subglacial hydrology, frontal plume melting and calving, J. Glaciol., 1–17, https://doi.org/10.1017/jog.2021.109, 2021a.

Cook, S. J., Christoffersen, P., Truffer, M., Chudley, T. R., and Abellán, A.: Calving of a Large Greenlandic Tidewater Glacier has Complex Links to Meltwater Plumes and Mélange, J. Geophys. Res. Earth Surf., 126, e2020JF006051, https://doi.org/10.1029/2020JF006051, 2021b.

Crawford, A., Åström, J., Benn, D. I., Luckman, A., Gladstone, R., Zwinger, T., Robertsén, F., and Bevan, S.: Calving Dynamics and the Potential Impact of Mélange Buttressing at the Western Calving Front of Thwaites Glacier, West Antarctica, J. Geophys. Res. Earth Surf., 129, e2024JF007737, https://doi.org/10.1029/2024JF007737, 2024.

Edwards, T. L., Nowicki, S., Marzeion, B., Hock, R., Goelzer, H., Seroussi, H., Jourdain, N. C., Slater, D. A., Turner, F. E., Smith, C. J., McKenna, C. M., Simon, E., Abe-Ouchi, A., Gregory, J. M., Larour, E., Lipscomb, W. H., Payne, A. J., Shepherd, A., Agosta, C., Alexander, P., Albrecht, T., Anderson, B., Asay-Davis, X., Aschwanden, A., Barthel, A., Bliss, A., Calov, R., Chambers, C., Champollion, N., Choi, Y., Cullather, R., Cuzzone, J., Dumas, C., Felikson, D., Fettweis, X., Fujita, K., Galton-Fenzi, B. K., Gladstone, R., Golledge, N. R., Greve, R., Hattermann, T., Hoffman, M. J., Humbert, A., Huss, M., Huybrechts, P., Immerzeel, W., Kleiner, T., Kraaijenbrink, P., Le clec'h, S., Lee, V., Leguy, G. R., Little, C. M., Lowry, D. P., Malles, J.-H., Martin, D. F., Maussion, F., Morlighem, M., O'Neill, J. F., Nias, I., Pattyn, F., Pelle, T., Price, S. F., Quiquet, A., Radić, V., Reese, R., Rounce, D. R., Rückamp, M., Sakai, A., Shafer, C., Schlegel, N.-J., Shannon, S., Smith, R. S., Straneo, F., Sun, S., Tarasov, L., Trusel, L. D., Van Breedam, J., van de Wal, R., van den Broeke, M., Winkelmann, R., Zekollari, H., Zhao, C., Zhang, T., and Zwinger, T.: Projected land ice contributions to twenty-first-century sea level rise, Nature, 593, 74–82, https://doi.org/10.1038/s41586-021-03302-y, 2021.

Fried, M. J., Catania, G. A., Stearns, L. A., Sutherland, D. A., Bartholomaus, T. C., Shroyer, E., and Nash, J.: Reconciling drivers of seasonal terminus advance and retreat at thirteen central west Greenland tidewater glaciers, J. Geophys. Res. Earth Surf., 0, https://doi.org/10.1029/2018JF004628, 2018.

Gagliardini, O. and Werder, M. A.: Influence of increasing surface melt over decadal timescales on land-terminating Greenland-type outlet glaciers, J. Glaciol., 1–11, https://doi.org/10.1017/jog.2018.59, 2018.

https://doi.org/10.5194/egusphere-2026-4213
Preprint. Discussion started: 27 July 2026

Gagliardini, O., Cohen, D., Råback, P., and Zwinger, T.: Finite-element modeling of subglacial cavities and related friction law, J. Geophys. Res. Earth Surf., 112, F02027, https://doi.org/10.1029/2006JF000576, 2007.

Gagliardini, O., Zwinger, T., Gillet-Chaulet, F., Durand, G., Favier, L., de Fleurian, B., Greve, R., Malinen, M., Martín, C., Råback, P., Ruokolainen, J., Sacchettini, M., Schäfer, M., Seddik, H., and Thies, J.: Capabilities and performance of Elmer/Ice, a new-generation ice sheet model, Geosci. Model Dev., 6, 1299–1318, https://doi.org/10.5194/gmd-6-1299-2013, 2013.

Goliber, S. A. and Catania, G. A.: Glacier Terminus Morphology Informs Calving Style, Geophys. Res. Lett., 51, e2024GL108530, https://doi.org/10.1029/2024GL108530, 2024.

Greene, C. A., Gardner, A. S., Schlegel, N.-J., and Fraser, A. D.: Antarctic calving loss rivals ice-shelf thinning, Nature, 609, 948–953, https://doi.org/10.1038/s41586-022-05037-w, 2022.

Greene, C. A., Gardner, A. S., Wood, M., and Cuzzone, J. K.: Ubiquitous acceleration in Greenland Ice Sheet calving from 1985 to 2022, Nature, 625, 523–528, https://doi.org/10.1038/s41586-023-06863-2, 2024.

Huth, A., Duddu, R., and Smith, B.: A Generalized Interpolation Material Point Method for Shallow Ice Shelves. 1: Shallow Shelf Approximation and Ice Thickness Evolution, J. Adv. Model. Earth Syst., 13, e2020MS002277, https://doi.org/10.1029/2020MS002277, 2021a.

Huth, A., Duddu, R., and Smith, B.: A Generalized Interpolation Material Point Method for Shallow Ice Shelves. 2: Anisotropic Nonlocal Damage Mechanics and Rift Propagation, J. Adv. Model. Earth Syst., 13, e2020MS002292, https://doi.org/10.1029/2020MS002292, 2021b.

Jiménez, S. and Duddu, R.: On the evaluation of the stress intensity factor in calving models using linear elastic fracture mechanics, J. Glaciol., 64, 759–770, https://doi.org/10.1017/jog.2018.64, 2018.

Joughin, I., Smith, B. E., and Howat, I. M.: A complete map of Greenland ice velocity derived from satellite data collected over 20 years, J. Glaciol., 64, 1–11, https://doi.org/10.1017/jog.2017.73, 2018.

Li, D., DeConto, R. M., and Pollard, D.: Climate model differences contribute deep uncertainty in future Antarctic ice loss, Sci. Adv., 9, eadd7082, https://doi.org/10.1126/sciadv.add7082, 2023.

Nick, F. M., Veen, C. J. V. D., Vieli, A., and Benn, D. I.: A physically based calving model applied to marine outlet glaciers and implications for the glacier dynamics, J. Glaciol., 56, 781–794, https://doi.org/10.3189/002214310794457344, 2010.

Seroussi, H., Pelle, T., Lipscomb, W. H., Abe-Ouchi, A., Albrecht, T., Alvarez-Solas, J., Asay-Davis, X., Barre, J.-B., Berends, C. J., Bernales, J., Blasco, J., Caillet, J., Chandler, D. M., Coulon, V., Cullather, R., Dumas, C., Galton-Fenzi, B. K., Garbe, J., Gillet-Chaulet, F., Gladstone, R., Goelzer, H., Golledge, N., Greve, R., Gudmundsson, G. H., Han, H. K., Hillebrand, T. R., Hoffman, M. J., Huybrechts, P., Jourdain, N. C., Klose, A. K., Langebroek, P. M., Leguy, G. R., Lowry, D. P., Mathiot, P., Montoya, M., Morlighem, M., Nowicki, S., Pattyn, F., Payne, A. J., Quiquet, A., Reese, R., Robinson, A., Saraste, L., Simon, E. G., Sun, S., Twarog, J. P., Trusel, L. D., Urruty, B., Van Breedam, J., van de Wal, R. S. W., Wang, Y., Zhao, C., and Zwinger, T.: Evolution of the Antarctic Ice Sheet Over the Next Three Centuries From an

https://doi.org/10.5194/egusphere-2026-4213
Preprint. Discussion started: 27 July 2026

ISMIP6 Model Ensemble, Earths Future, 12, e2024EF004561, https://doi.org/10.1029/2024EF004561, 2024.

Slater, D. A., Goldberg, D. N., Nienow, P. W., and Cowton, T. R.: Scalings for Submarine Melting at Tidewater Glaciers from Buoyant Plume Theory, J. Phys. Oceanogr., 46, 1839–1855, https://doi.org/10.1175/JPO-D-15-0132.1, 2016.

Todd, J., Christoffersen, P., Zwinger, T., Råback, P., Chauché, N., Benn, D., Luckman, A., Ryan, J., Toberg, N., Slater, D., and Hubbard, A.: A Full-Stokes 3D Calving Model applied to a large Greenlandic Glacier, J. Geophys. Res. Earth Surf., 2017JF004349, https://doi.org/10.1002/2017JF004349, 2018.

Walter, A., Lüthi, M. P., and Vieli, A.: Calving event size measurements and statistics of Eqip Sermia, Greenland, from terrestrial radar interferometry, The Cryosphere, 14, 1051–1066, https://doi.org/10.5194/tc-14-1051-2020, 2020.

Weidick, A.: Greenland, Department of the Interior, U.S. Geological Survey, 160 pp., 1995.

Werder, M. A., Hewitt, I. J., Schoof, C. G., and Flowers, G. E.: Modeling channelized and distributed subglacial drainage in two dimensions, J. Geophys. Res. Earth Surf., 118, 2140–2158, https://doi.org/10.1002/jgrf.20146, 2013.

van Wessem, J. M., Berg, W. J. van de, Noël, B. P. Y., Meijgaard, E. van, Amory, C., Birnbaum, G., Jakobs, C. L., Krüger, K., Lenaerts, J. T. M., Lhermitte, S., Ligtenberg, S. R. M., Medley, B., Reijmer, C. H., Tricht, K. van, Trusel, L. D., Ulft, L. H. van, Wouters, B., Wuite, J., and Broeke, M. R. van den: Modelling the climate and surface mass balance of polar ice sheets using RACMO2 – Part 2: Antarctica (1979–2016), The Cryosphere, 12, 1479–1498, https://doi.org/10.5194/tc-12-1479-2018, 2018.

Wheel, I., Benn, D. I., Crawford, A. J., Todd, J., and Zwinger, T.: A new 3D full-Stokes calving algorithm within Elmer/Ice (v9.0), Geosci. Model Dev., 17, 5759–5777, https://doi.org/10.5194/gmd-17-5759-2024, 2024a.

Wheel, I., Crawford, A. J., and Benn, D. I.: Calving dynamics at Jakobshavn Isbrae (Sermeq Kujalleq) controlled by local geometry: insights from a 3D Stokes calving model, J. Glaciol., 70, e7, https://doi.org/10.1017/jog.2024.77, 2024b.

Wheel, I., Benn, D. I., and Crawford, A. J.: Emergent Dynamics From a Position-Based Calving Function and the Limits of a Rate-Based Calving Function, J. Geophys. Res. Earth Surf., 131, e2025JF008631, https://doi.org/10.1029/2025JF008631, 2026.

Wheel, I., Cook, S.J., Benn, D.I., Crawford, A.J., and Luckman, A.: Modelling stochastic calving at Jakobshavn Isbrae (Sermeq Kujalleq) and Store Glacier (Sermeq Kujalleq), Nature Geoscience (in prep.)

Xie, S., Dixon, T. H., Holland, D. M., Voytenko, D., and Vaňková, I.: Rapid iceberg calving following removal of tightly packed pro-glacial mélange, Nat. Commun., 10, 3250, https://doi.org/10.1038/s41467-019-10908-4, 2019.

Yu, H., Rignot, E., Morlighem, M., and Seroussi, H.: Iceberg calving of Thwaites Glacier, West Antarctica: full-Stokes modeling combined with linear elastic fracture mechanics, The

https://doi.org/10.5194/egusphere-2026-4213
Preprint. Discussion started: 27 July 2026

Cryosphere, 11, 1283–1296, https://doi.org/10.5194/tc-11-1283-2017, 2017.